ACS Catalysis

RESEARCH ARTICLE

pubs.acs.org/acscatalysis

Thermodynamic Cartography and Structure/Property Mapping of Commercial Platinum Catalysts

Amanda S. Barnard*,† and Lan Y. Chang‡

†CSIRO Materials Science and Engineering, Clayton, Victoria, 3168 Australia and

‡Monash Centre for Electron Microscopy and School of Chemistry, Monash University, Clayton, Australia

Supporting Information

ABSTRACT: The development of the next generation of nanosized heterogeneous catalysts requires precise control of the size, shape, and structure of individual components in a variety of chemical environments. Recent reports show that the density of catalytically active defects on Pt nanoparticles is intrinsically linked to performance, such as edges, corners, steps, and kinks, which may be introduced postsynthesis. To optimize the synthesis of nanoparticles decorated by these defects and to understand the structural stability of the final product, multiscale thermodynamic modeling has been used to predict the size and temperature dependence of these steps and to show how this directly relates to catalytic reactivity. The results show that relatively modest annealing can promote the formations of surface steps and kinks and can more than double the reactivity of particles at industrially relevant sizes.

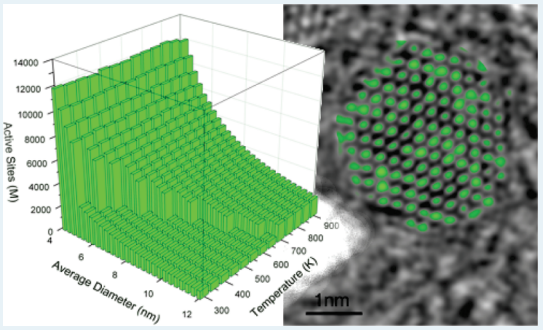

KEYWORDS: heterogeneous catalyst, active defects, edges, corners, steps, kinks, thermodynamic cartography, Pt nanoparticles

The solution to our ever increasing energy needs comes in three parts: reducing consumption, utilizing renewable sources, and increasing efficiency (irrespective of the source). The introduction of biofuels to replace existing fossil fuels is one option that has the advantage of alleviating much of the cost associated with an entire change of infrastructure and will likely return positive results in a short period of time.[1] However, irrespective of whether fossil fuels, biofuels, or some other alternatives are used, it is still currently necessary to catalyze the reaction to harness the energy for many applications. To date, the most efficient heterogeneous catalysts in modern fuel cells are dispersed platinum (or Pt-alloy) nanoparticles supported on carbon, aluminum oxide, or titanium oxide.[2,3] One of the most important applications for Pt is as a catalytic converter (in the automotive industry) because it facilitates the complete combustion of low concentrations of unburned hydrocarbons from the exhaust. However, platinum is extremely rare, occurring in only <0.003 ppb in the earth's crust.

To improve the economic sustainability of this technology, we must find intelligent ways of reducing the amount of Pt needed, increasing the number of cycles each catalyst can perform (recyclability) and increasing efficiency by controlling the number of catalytically active sites (per particle). Nanosized heterogeneous catalysts show a considerably different catalytic activity and reactivity from macroscopic (planar) materials,[4,5] but recent evidence suggests that these changes include fundamental physical and chemical changes at the active sites in addition to the obvious increase in surface area.[6−9] In particular, the shape of individual nanoparticles has an important influence on efficiency due to anisotropic adsorption of reactants at the exposed surface facets.[10] For example, benzene hydrogenation has been investigated in the presence of a surface monolayer consisting of cubic and cuboctahedral Pt nanoparticles and it has been shown that cyclohexane and cyclohexene product molecules were formed on cuboctahedral nanoparticles, whereas only cyclohexane was produced on cubic nanoparticles.[11] Moreover, CO monolayer oxidation on quasi-spherical, cubic, and tetrahedral−hexagonal platinum nanoparticles revealed a clear dependence between bidimensional (111) and (100) ordered domains present on the surface of the nanoparticles and their CO catalytic activity.[12]

It is now widely understood that controlling the intrinsic structural properties of the Pt nanoparticles is imperative to optimizing their catalytic properties,[13,14] and studies accessing finer resolutions have determined that (in addition to shape) catalytic properties and selectivity depends sensitively on the presence and density of surface defects.[10,15] By increasing the fraction of active sites (such as edges, corners, and surface defects), the surface reactivity of Pt particles may be increased, but the same procedure will decrease catalytic activity, which is related to the rate-determining step (RDS) of the reaction of specific reactions. This is will be beneficial in the case of bond-breaking reactions, but detrimental for bond-making reactions,

Received: September 30, 2010
Revised: November 24, 2010
Published: January 14, 2011

in which a lower surface reactivity is required. Advanced characterization techniques have been use to clarify the role of active sites on the extended surfaces of model catalysts[16] and to provide atomic-resolution information regarding local topologies of these sites on nanoparticles that are already commercially available.[17,18] The later has been obtained using high-resolution transmission electron microscopy (HRTEM), which combines spherical-aberration correction[19] and exit wave function restoration,[20,21] that together provide greater sensitivity than has been possible in the past.[22]

These new methods have enabled detailed studies of the structure of different types of defects on the surface of these nanosized heterogeneous catalysts. Commercial catalysts used to reduce O_2 at the cathodes and oxidize H_2 at the anodes of polymer electrolyte membrane fuel cells typically present as truncated octahedra, as evidenced by electron tomography results on the rough shape of these particles,[23] and the surfaces may be decorated with different types of steps and kinks.[24] When present, these imperfect surfaces, along with the edges and corners characteristic of the three-dimensional shape, enhance the efficiency of the catalysts because the severely reduced coordination of the atoms at these sites offers an increased number of reaction sites.

During the processing of these materials, it is customary to pretreat a sample by heating to allow for structural equilibration. This is typically performed in a H_2 or N_2 gaseous environment,[17,22] depending upon the temperature used during treatment. It is assumed that this treatment increases the number of active sites (steps, kinks, edges, and corners), but this has not been quantified, and to date, no size- and temperature-dependent structure/property map exists. Development of such a structure/property map is highly desirable because it assists in the manufacture of more efficient catalysts; however, this is a very challenging and expensive undertaking if restricted to HRTEM imaging of conventional samples.

Therefore, we will use an established theoretical nanomorphology model and results from accurate first principles computer simulations to generate the first structure/property map for predicting the pretreatment required to increase the number of active sites on Pt nanoparticle and, therefore, engineer more efficient catalysts. We begin by mapping the equilibrium shape and structure as a function of size and temperature (thermodynamic cartography) and then project the numerical summation of active edge, corner, step, and kink sites as a measure of reactivity.

METHODS

The shape-dependent model used here is based on a summation of the Gibbs free energy $G(T)$ of a nanoparticle and includes contributions from the particle bulk, surfaces, edges, corners, and planar defects.[25] This model has previously been successfully used to examine the size- and temperature-dependent shape of gold nanoparticles and nanorods without necessitating a large number of explicitly simulations of individual structures.[26−28] Here, since we are concerned with nanoparticles >3 nm in diameter that do not contain planar defects, we may use the expression

$$G(T) = \Delta G_f^0(T) + \frac{M}{\rho}\left(1 - \frac{2\sum_i f_i\,\sigma_i(T)}{B_0\langle R\rangle} + \frac{P_{ex}}{B_0}\right)\left[q\sum_i f_i\gamma_i(T)\right] \quad (1)$$

where M is the molar mass, ρ is the mass density, q is the surface to volume ratio, f_i is the fractional area weighting factor, and $\gamma_i(T)$ is the temperature-dependent free energy of facet i. The volume dilation induced by the isotropic surface stresses, σ_i, and external pressure, P_{ex}, is included using the Laplace−Young formalism[25] using the bulk modulus, B_0, and the average particle radius, $\langle R\rangle$, calculated using a spherical approximation (which is consistent with the Laplace−Young formalism). In all cases, atmospheric external pressure has been assumed (P_{ex} = 101.33 kPa).

The version of the model requires the input of B_0, $\gamma_i(T)$, and $\sigma_i(T)$, which must be calculated explicitly for all facets, i, of interest. The calculations performed in this study were performed from first principles using density functional theory (DFT) within the generalized gradient approximation (GGA), with the exchange correlation functional of Perdew−Burke−Ernzerhof (PBE).[29] This has been implemented via the Vienna ab initio simulation package (VASP).[30,31] All calculations were performed using the projected augmented wave (PAW) potentials[32,33] to an energy convergence of 10^{-4} eV using periodic supercells separated by thick vacuum space layers. Each structure was relaxed prior to accurate static single point energy calculations. More information on the supercell structures and the simulation methods can be found in the Supporting Information. This provides values of $\gamma_{111,step}$ = 1.33 J/m^2, γ_{111} = 1.26 J/m^2, $\gamma_{100,step}$ = 1.77 J/m^2, γ_{100} = 1.72 J/m^2, γ_{110} = 1.78 J/m^2; $\sigma_{111,step}$ = 5.87 J/m^2, σ_{111} = 5.41 J/m^2, $\sigma_{100,step}$ = 2.91 J/m^2, σ_{100} = 3.40 J/m^2, σ_{110} = 2.01 J/m^2, and B_0 = 2.76 GPa. Although a detailed comparison of these results with other DFT and experimental studies can be found in the Supporting Information, (as a guide) the {111} step formation energy was found to be 0.26 eV/atom, which is in good agreement with the value of 0.25 eV/atom calculated by Boisvert, Lewis, and Scheffler using the same equation and k-point sampling (as reported in reference 34).

Since these DFT calculations have been performed at $T \approx 0$, a number of simple expressions, which have previously been shown to be suitable for this type of analysis,[26] have been used here to describe the temperature dependence. First, we have used a semiempirical expression for determining of $\gamma_i(T)$ proposed by Guggenheim:[35]

$$\gamma_i(T) = \gamma_i(0)\left(1 - \frac{T}{T_c}\right)^x \quad (2)$$

where x is an empirical parameter (known to be unity for metals[36]) and T_c is the critical temperature at which the structure of the surface deteriorates or changes significantly from the structure in the bulk (is no longer fcc).[37] The value of T_c is usually taken as the bulk surface melting temperature, but since this has been shown to be size-dependent in metallic nanoparticles,[38] the expression of Qi and Wang[39] has also been employed,

$$T_c = T_m\left(1 - \frac{6r\Omega}{D}\right) \quad (3)$$

where T_m is the macroscopic surface melting temperatures, D is the average diameter of the nanostructure, r is the atomic radius of platinum, and Ω is a shape-dependent factor defined as the ratio of the surface area of the particle divided by the surface area of a sphere of equivalent volume.[39] Since $\sigma = \gamma + A\,\partial\gamma/\partial A$, the temperature dependence of σ_i has been described in the same way, as has been rigorously validated for metallic nanoparticles in reference 40.

dx.doi.org/10.1021/cs100025y |ACS Catal. 2011, 1, 76–81

DISCUSSION OF RESULTS

This method has previously been proven successful in describing the temperature-dependent shape, stability, and transformation in gold nanoparticles,[40] but in previous work, all surface facets have been flat. Although the values of $\gamma_i(0)$ can be easily calculated for stepped surfaces (see the Supporting Information), the value of T_m will be different. In the case of stepped surfaces, $T_{m,step}$ will be a combination of the surface melting temperature of the flat surface and the kink activation temperature, which is derived from the surface mass diffusion in accordance with the Nernst−Einstein equation (which determines the flux of surface atoms that flows in response to a driving chemical potential gradient). This was investigated in the range 710−1220 K by Rajappan et al,[41] who measured surface mass diffusion coefficients from the decay of Fourier components observed by low-energy electron microscopy. Their results agreed with previously reported values obtained from step fluctuation spectroscopy and combined to give diffusion coefficient of $D_s = 4 \times 10^{-3}$ exp$(-1.47\ \text{eV}/k_BT)$ cm^2 s^{-1}.

This means that $T_{m,step}$ will be a function of the terrace + kink density, but to facilitate a direct comparison with pristine particles (without kinks and terraces), we require that the number of atoms be constant. Therefore, on the basis of the experimental observations, we recognize the introduction of steps on the particle surfaces is accompanied by the introduction of new {110} facets on these particles, and we assume that the two observations are correlated. Platinum atoms initially residing on the high-energy {111}|{111} edges diffuse to the {111} surfaces during the pretreatment of these samples. Hence, we assign the terrace + kink density of the stepped nanoparticle to be equivalent to the number of atoms that would occupy the edge sites if the particle was pristine and remove the edges (exposing {110} facets) simultaneously. As the size of the nanoparticle increases, the number of edge atoms on the equivalent pristine structures increases, and therefore, the number of number of terrace and kink atoms on the stepped particles increases.

The number of edge atoms will also change with shape, and the shape ({111}-to-{100} ratio) of a stepped nanoparticle may differ from a pristine one, so the number of atoms participating in this defect is solved self-consistently. Results showing the change in shape for pristine and stepped Pt nanocatalysts as a function of size are shown in Figure 1 at a temperature of 300 K. We can see that, irrespective of the presence of surface steps, the equilibrium shape is dominated by {111} facets and the fraction of {111} facet converge at 32 nm (within the resolution of the model). This is in excellent agreement with the shapes observed experimentally.[24] Examples of the our nanoparticles showing the shape and surface defects are also shown in Figure 1b, c, and d at 3, 6, and 8 nm, respectively. These nanoparticles have been subjected to postsynthesis treatment by the manufacturer, which involves heating to 900 °C in a N_2-rich atmosphere, to increase the density of surface defects.[22] At this point, it should be noted that although the model has been used to optimize the shape here, any nonequilibrium (kinetically produced) shapes may be input and used in the following analysis.

By repeating these size-dependent shape optimizations for a range of temperatures, a prediction of the free energy of formation G can be determined at a function of both D and T. These have been formed in the range $D = 3-27$ nm, and $T = 0-1000$ K and are presented for the pristine and stepped Pt nanocatalysts in Figure 2a and b, respectively. Alternative configurations with stepped {111} surface and planar {100} surfaces, or planar {111} surfaces and stepped {100} surfaces, were also considered in the same way. All types of particles exhibit a $1/D$ decrease in energy with increasing size, and evidence of the melting point depression can be seen (as $G < 0$) for small stepped particles <5 nm at high temperatures >700 K. At this point, we highlight that it is also possible to find the lowest energy (thermodynamically preferred) *size* for a given *shape*; however, this is not as useful in this context, since particle size is the product criteria provided by many manufacturers. In reality, however, both the average particle diameter and the particle shape can be directly controllable conditions via particle engineering during synthesis.[44−46]

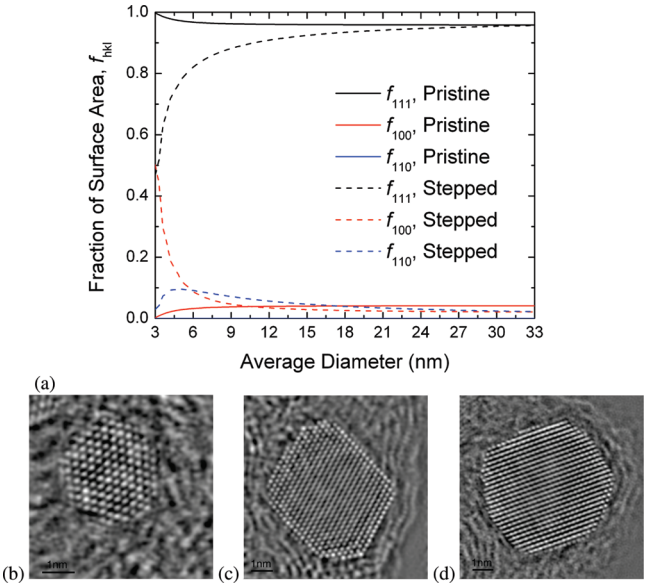

Figure 1. (a) Predicted shape of platinum nanoparticles with pristine (planar) surfaces and stepped surfaces as a function of size at 300 K and a set of exemplary experimental phase images restored from HRTEM focal series of a (b) 3, (c) 6, and (c) 8 nm [110]-oriented carbon-supported commercial platinum heterogeneous catalyst taken at 200 kV, with spherical aberration C_s adjusted to −30 μm (focus = 65.2 nm). Postsynthesis treatment by the manufacturer involves heating to 900 °C in a N_2-rich atmosphere.[22].

Since each of the data points along the curves in Figure 2 has been modeled at the same size, these results are directly comparable, and the relative thermodynamic stability of stepped and pristine nanocatalysts can be determined. This has been done here, and the results projected onto the $\langle D,T\rangle$ plane, thereby producing a stability mapping referred to as thermodynamic cartography, as shown in Figure 3. This map predicts the preferred structure at each each point in $\langle D, T\rangle$ space, since both the selectivity between stepped, pristine and combinations stepped/pristine particles is presented and the nanomorphology of each alternative at all points is known. Readers will note that the region between the black (solid symbol) and red (open symbol) curves predicts the regime for particles with stepped {111} surface and planar {100} surfaces.

On the basis of these structural predictions, we can then define the structure/property map for catalytic reactivity by simply counting the number of active sites on each structure at each point below the melting temperature (see Figure 4). Above the melting temperature, this is not possible, since the crystallinity

dx.doi.org/10.1021/cs100025y |*ACS Catal.* 2011, 1, 76–81

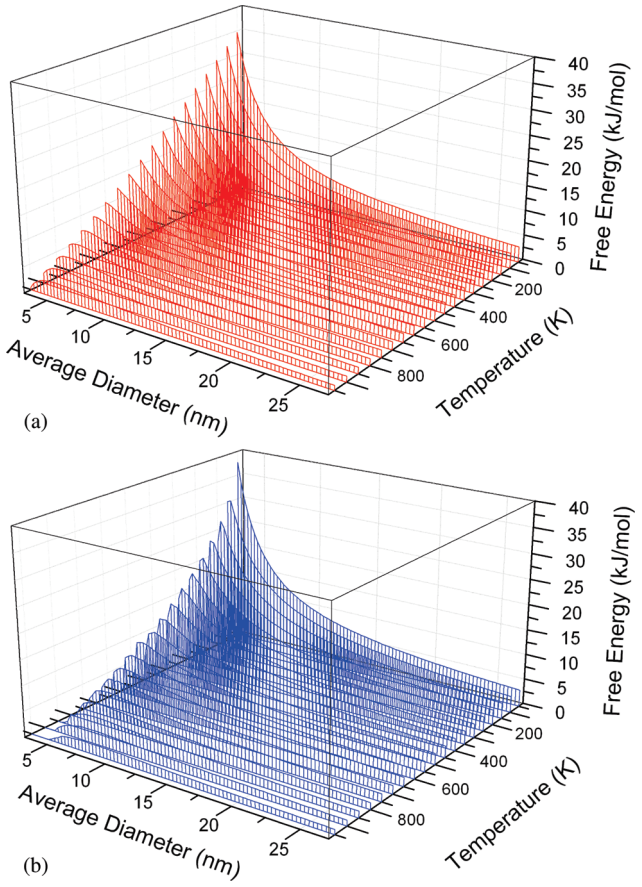

Figure 2. Predicted free energy of formation in the range $D = 3-27$ nm, and $T = 0-900$ K for nanoparticles with (a) a pristine planar surface. (b) Stepped surfaces are shown in Figure 1b.

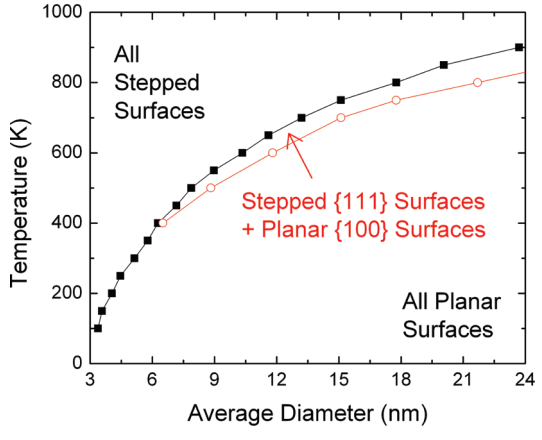

Figure 3. Thermodynamic cartography of platinum nanoparticles, predicting the preferred structure in $\langle D,T \rangle$ space. Results account for size- and temperature-dependent changes in shape as well as associated changes in surface defect density. The region between the black (solid symbol) and red (open symbol) curves predicts the regime for particles with a stepped {111} surface and pristine planar {100} surfaces.

and the geometry of the particles are no longer preserved. Figure 4 shows that, in agreement with numerous experimental studies reported in the literature, there is a dramatic increase in the molar number of active sites as the size of the particles

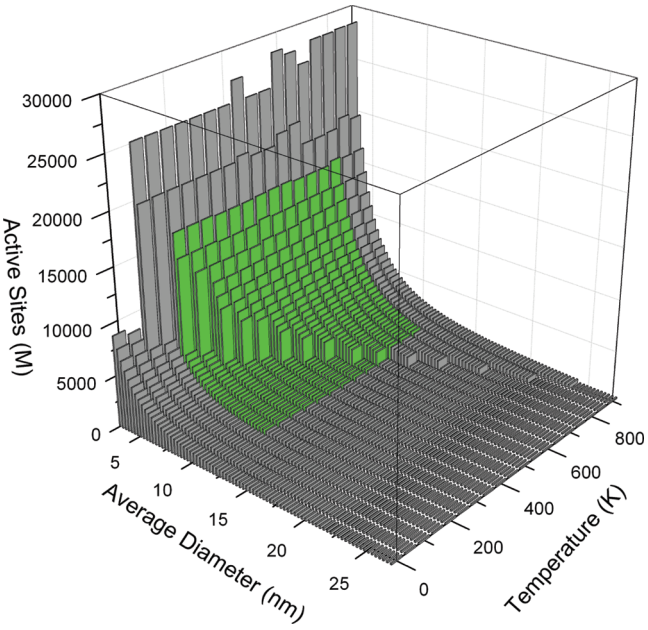

Figure 4. Structure/property map of the catalytic reactivity of platinum heterogeneous catalysts, based on the thermodynamic cartography presented in Figure 3 when reactivity is restricted to under-coordinated edges, corners, steps, and kinks, with the industrially relevant range of $D = 3.5-12.5$ nm and $T = 300-800$ K highlighted in green.

decreases. Although we are accustomed to relating this to the surface-to-volume ratio (which is proportional to $1/D$), this trend is more closely related to the edge/step-to-volume ratio (which is proportional to $1/D^2$) and the corner/kink-to-volume ratio (which is proportional to $1/D^3$).

The reactivity of larger nanoparticles is improved by thermal annealing that introduces surface defects, but the results converge at $\langle 27$ nm, 900 K$\rangle$. This is consistent with experimental observations, which have revealed that the average reaction rate increases exponentially with the increase in percentage of surface atoms on edges and corners of faceted Pt nanocrystals.[42] Variations in reactivity of small nanoparticles at high temperatures are evident due to shape fluctuations in the vicinity of the (critical) melting point. Readers will note that the region between the black (solid symbol) and red (open symbol) curves of Figure 3 predicts the regime for particles with a stepped {111} surface and planar {100} surfaces, but this does not invoke a discernible fluctuation in the property map, since the fraction of {100} surface areas is very small at these sizes (see Figure 1a).

The most important aspect of this structure property map is in the range 3.5−12.5 nm, which is the size typical of commercial samples,[43] as highlighted in Figure 4. In this range, we can see that the introduction of steps more than doubles the number of active sites and can therefore be expected to double the catalytic reactivity, where bond breaking is required.[47,48] For example, Gambardella et al.[15] used a combination of scanning tunneling microscopy, thermal energy atom scattering, and density functional theory to show how the dissociation of O_2 on Pt(111) is enhanced on stepped surfaces. They found that the increased reactivity at the Pt step sites is not caused by a decrease in the local dissociation barriers from the molecular precursor state, but was instead related to a stabilization of both the molecular precursor state and transition state. This is in contrast to other materials, such as ruthenium.[49] In both the molecular precursor

dx.doi.org/10.1021/cs100025y |ACS Catal. 2011, 1, 76–81

state and the transition state, the O_2 has its axis aligned parallel to the step edge, and the reactivity of Pt step sites could be locally tuned via controlled step decoration with Ag monatomic chains.

This map also simultaneously provides a prediction of the decrease in potential catalytic activity (as mentioned above), where bond-making reactions are required.[44] Following annealing, it is reasonable to expect that this increase in active sites could be maintained, since it has been reported that the deactivation of Pt nanocatalysts is the result of a decrease in the concentration of surface intermediates (as a result of carbon deposition), as opposed to changes in the intrinsic site activity.[50] The behavior of molecules in the proximity of kinks and steps is critical to our understanding chemisorption processes on catalytic surfaces,[37,49] so the next stage in this study is to determine how the structure/property map is likely to change in response to the presence of different surface adsorbates. This is a topic of ongoing work.

On a final note, it is prudent to point out that the present study has restricted the morphologies to those consistent with our experimental samples, but considerable attention is being directed to engineering alternative shapes to increase (or decrease) reactivity.[46] The effects of particle shapes on catalytic performance were first reported by Narayanan and El-Sayed,[42,51−54] in which cubic, truncated octahedral, and tetrahedral platinum nanocrystals were investigated for the electron transfer reaction between $[Fe(CN)_6]^{3-}$ and $S_2O_3^{2-}$ ions. It was found that the percentage of atoms located at corners and edges relative to the total surface atoms was highest for tetrahedral nanocrystals, followed by truncated octahedral and cubic nanocrystals, which leads to a decrease in the catalytic activity of cubic shapes (or conversely, an increase in reactivity).[53,54] In regard to fuel cell applications, it has also been demonstrated that the specific activity of cubic platinum nanocrystals for oxygen reduction reaction can be as much as 4 times higher than those of truncated cubic and near-spherical polyhedral nanocrystals,[55] and up to twice the activity of the commercial catalyst,[56] such as those considered here. We therefore intend to pursue this topic in the near future and estimate the role of surface steps and kinks on the performance of tetrahedral, cubic, and other alternative morphologies.

CONCLUSION

In summary, using a size- and shape-dependent theoretical model, we have performed the thermodynamic cartography of platinum nanoparticle heterogeneous catalysts, including the effects of temperature and the presence of surface defects, such as those observed in commercial samples. We find that the preferred shape is truncated octahedron (dominated by {111} facets), independent of whether the surfaces include steps and kinks, but defective surfaces are energetically preferred at higher temperatures. This is more pronounced at small sizes and is due to the reduction of the surface melting temperature, as determined self-consistently using the kink activation temperature and the defect density. The stepped nanoparticles also contain {110} facets, in agreement with experiment, and therefore exhibit a much higher number of edge and corner atoms, in addition to the step and kink atoms, which more than doubles the number of active sites available for catalytic reactions.

The active sites considered in this study will also be available to other types of (noncatalytic) reactions, such as generation or suppression of toxic free radicals. Although the surfaces of other fcc metal nanoparticles have been shown to be efficient generators of reactive oxygen species,[57] platinum has been suggested as an antioxidant and efficient scavenger of superoxide anion and hydroxyl radicals.[58] Depending upon one's perspective, the technique used here is also a predictor of these undesirable or desirable environmental interactions.

These results therefore predict how sensitive control of annealing temperature may be used to improve the efficiency of as-synthesized platinum nanoparticles or how in situ temperatures characteristic of catalytic converters may influence performance. Using this structure/property map and using the thermodynamic cartography method reported here, new predictions of heterogeneous catalysis can lead to better control of the chemical reactions and may result in the rational design of better catalysts.

ASSOCIATED CONTENT

Supporting Information. Additional information as noted in text. This material is available free of charge via the Internet at http://pubs.acs.org.

AUTHOR INFORMATION

Corresponding Author
*E-mail: amanda.barnard@csiro.au.

ACKNOWLEDGMENT

This project has been supported by L'Oréal Australia, Mercedes-Benz and the Banksia Environmental Foundation, and the Australian Research Council under Grant No. DP0986752. Computational resources for this project have been supplied by the National Computing Infrastructure (NCI) national facility under MAS Grant p00, and the nEO shape modeling software was prepared by Dr. Matthew Matin.

REFERENCES

(1) Hill, J.; Nelson, E.; Tilman, D.; Polasky, S.; Tiffany, D. *Proc. Natl. Acad. Sci. U.S.A.* **2006**, *103*, 11206.
(2) Suchorski, Y.; Drachsel, W. *Top. Catal.* **2007**, *46*, 201.
(3) *Catalysis and Electrocatalysis at Nanoparticle Surfaces*; Wieckowski, A., Savinova, E. R., Vayenas, C. G., Eds.; Dekker: New York, 2003; pp 455−500.
(4) Meier, J.; Friedrich, K. A.; Stimming, U. *Faraday Discuss.* **2002**, *121*, 365.
(5) Yano, H.; Inukai, J.; Uchida, H.; Watanabe, M.; Babu, P. K.; Kobayashi, T.; Chung, J. H.; Oldfield, E.; Wieckowski, A. *Phys. Chem. Chem. Phys.* **2006**, *8*, 4932.
(6) Hammer, B.; Nørskov, J. K. *Adv. Catal.* **2000**, *45*, 71.
(7) Lopez, N.; Nørskov, J. K. *J. Am. Chem. Soc.* **2002**, *124*, 11262.
(8) Mayrhofer, K. J. J.; Blizanac, B. B.; Arenz, M.; Stamenkovic, V. R.; Ross, P. N.; Markovic, N. M. *J. Phys. Chem. B* **2005**, *109*, 14433.
(9) Arenz, M.; Mayrhofer, K. J. J.; Stamenkovic, V.; Blizanac, B. B.; Tomoyuki, T.; Ross, P. N.; Markovic, N. M. *J. Am. Chem. Soc.* **2005**, *127*, 6819.
(10) Mayrhofer, K. J. J.; Arenz, M.; Blizanac, B. B.; Stamenkovic, V.; Ross, P. N.; Markovic, N. M. *Electrochim. Acta* **2005**, *50*, 5144.
(11) Bratlie, K. M.; Lee, H.; Komvopoulos, K.; Yang, P.; Somorjai, G. A. *Nano Lett.* **2007**, *7*, 3097.
(12) Solla-Gullón, J.; Vidal-Iglesias, F. J.; Herrero, E.; Feliu, J. M.; Aldaz, A. *Electrochem. Commun.* **2006**, *8*, 189.
(13) Harris, P. J. F. *Int. Mater. Rev.* **1995**, *40*, 97.
(14) Ahmadi, T. S.; Wang, Z. L.; Green, T. C.; Henglein, A.; El-Sayed, M. A. *Science* **1996**, *272*, 1924.
(15) Gambardella, P.; Sljivančanin, Ž.; Hammer, B.; Blanc, M.; Kuhnke, K.; Kern, K. *Phys. Rev. Lett.* **2001**, *87*, 056103.

(16) Honkala, K.; Hellman, A.; Remediakis, I. N.; Logadottir, A.; Carlsson, A.; Dahl, S.; Christensen, C. H.; Nørskov, J. K. *Science* **2005**, *307*, 555.
(17) Ralph, B. T. R.; Hogarth, M. P. *Platinum Met. Rev.* **2002**, *46*, 3.
(18) Datye, A. K.; Logan, A. D.; Blankenburg, J.; Smith, D. J. *Ultramicroscopy* **1990**, *34*, 47.
(19) Haider, M.; Rose, H.; Uhlemann, S.; Schwan, E.; Kabius, B.; Urban, K. *Ultramicroscopy* **1998**, *75*, 53.
(20) Kirkland, A. I.; Meyer, R. R. *Microsc. Microanal.* **2004**, *10*, 401.
(21) Chang, L. Y.; Kirkland, A. I. *Microsc. Microanal.* **2006**, *12*, 469.
(22) Gontard, L. C.; Chang, L.-Y.; Hetherington, C. J. D.; Kirkland, A. I.; Ozkaya, D.; Dunin-Borkowski, R. E. *Angew. Chem., Int. Ed.* **2007**, *46*, 3683.
(23) Gontard, L. C.; Dunin-Borowski, R. E.; Ozkaya, D. *J. Microsc.* **2008**, *232*, 248.
(24) Chang, L.-Y.; Barnard, A. S.; Gontard, L. C.; Dunin-Borkowski, R. E. *Nano Lett.* **2010**, *10*, 3073.
(25) Barnard, A. S. *J. Phys. Chem. B* **2006**, *110*, 24498.
(26) Barnard, A. S.; Lin, X. M.; Curtiss, L. A. *J. Phys. Chem. B* **2005**, *109*, 24465.
(27) Barnard, A. S.; Curtiss, L. A. *J. Mater. Chem.* **2007**, *17*, 3315.
(28) Barnard, A. S. *J. Phys. Chem. B* **2008**, *112*, 1385.
(29) Perdew, J. P.; Burke, K; Ernzerhof, M. *Phys. Rev. Lett.* **1996**, *77*, 3865.
(30) Kresse, G.; Hafner, J. *Phys. Rev. B* **1993**, *47*, RC558.
(31) Kresse, G.; Furthmüller, J. *Phys. Rev. B* **1996**, *54*, 11169.
(32) Blöchl, P. E. *Phys. Rev. B* **1994**, *50*, 17953.
(33) Kresse, G.; Joubert, D. *Phys. Rev. B* **1999**, *59*, 1758.
(34) Boisvert, G.; Lewis, L. J.; Scheffler, M. *Phys. Rev. B* **1998**, *57*, 1881.
(35) Guggenheim, E. A. *Thermodynamics*, 4th ed.; North Holland: Amsterdam, The Netherlands, 1993.
(36) Grosse, A. V. *J. Inorg. Nucl. Chem.* **1962**, *24*, 147.
(37) Somorjai, G. A. *Introduction to Surface Chemsitry and Catalysis*; John Wiley & Sons, Inc.: New York, 1994.
(38) Buffat, Ph.; Borel, J.-P. *Phys. Rev. A* **1976**, *13*, 2287.
(39) Qi, W. H.; Wang, M. P. *Mater. Chem. Phys.* **2004**, *88*, 280.
(40) Barnard, A. S.; Young, N.; Kirkland, A. I.; van Huis, M. A.; Xu, H. *ACS Nano* **2009**, *3*, 1431.
(41) Rajappan, M.; Swiech, W.; Ondrejcek, M.; Flynn, C. P. *J. Phys.: Condens. Matter* **2007**, *19*, 226006.
(42) Narayanan, R.; El-Sayed, M. A. *Nano Lett.* **2004**, *4*, 1343.
(43) Ozkaya, D.; Thompsett, D.; Goodlet, G.; Spratt, S.; Ash, P.; Boyd, D. *Inst. Phys. Conf. Ser.* **2003**, *179*, 2.
(44) Peng, Z.; Yang, H. *Nano Today* **2009**, *4*, 143.
(45) Sau, T. K.; Rogach, A. L. *Adv. Mater.* **2010**, *22*, 1781.
(46) Cheong, S.; Watt, J. D.; Tilley, R. D. *Nanoscale* **2010**, *2*, 2045.
(47) Gland, J. L.; Sexton, B. A.; Fisher, G. B. *Surf. Sci.* **1980**, *93*, 487.
(48) Winkler, A.; Guo, X.; Siddiqui, H. R.; Hagans, P. L.; Yates, J. T., Jr. *Surf. Sci.* **1988**, *201*, 419.
(49) Zambelli, T.; Wintterlin, J.; Trost J.; Ertl, G. *Science*, **1996**, *273*, 1688.
(50) Sirijaruphan, A.; Goodwin, J. G., Jr.; Rice, R. W. *J. Catal.* **2004**, *221*, 288.
(51) Narayanan, R.; El-Sayed, M. A. *J. Phys. Chem. B* **2003**, *107*, 12416.
(52) Narayanan, R.; El-Sayed, M. A. *J. Am. Chem. Soc.* **2004**, *126*, 7194.
(53) Narayanan, R.; El-Sayed, M. A. *J. Phys. Chem. B* **2004**, *108*, 5726.
(54) Narayanan, R.; El-Sayed, M. A. *Langmuir* **2005**, *1*, 2027.
(55) Wang, C.; Daimon, H.; Onodera, O.; Koda, T.; Sun, S. *Angew. Chem., Int. Ed.* **2008**, *47*, 3588.
(56) Wang, C.; Daimon, H.; Lee, Y.; Kim, J.; Sun, S. *J. Am. Chem. Soc.* **2007**, *129*, 6974.
(57) Akdim, B.; Hussain, S.; Pachter, R. In *Proceedings of the 8th International Conference on Computational Science, Lecture Notes in Computational Science, Part II*; Burbak, M., Albada, G. D., van Dogara, J., Sloot, P. M. A., Eds; Springer: Berlin, 2008; Vol. *5102*, pp 353−359.
(58) Hamasaki, T.; Kashiwagi, T.; Imada, T.; Nakamichi, N.; Aramaki, S.; Toh, K.; Morisawa, S.; Shimakoshi, H.; Hisaeda, Y.; Shirahata, S. *Langmuir* **2008**, *24*, 7354.